Velocity-matching model for electron capture in keV atomic collisions

Emil Y. Sidky and Hans-Jørgen T. Simonsen
Ørsted Laboratory, University of Copenhagen, Universitetsparken 5, DK-2100 Copenhagen Ø, Denmark
(Received 17 January 1996; revised manuscript received 16 April 1996)

We develop an approximate integral for the amplitudes of electron transfer in ion-atom collisions. The resulting model pertains to collisions involving low-*n* excited states and relative ion-atom velocities near the average speed of the target valence electron. Three points are essential to the derivation: (1) the atomic states are treated as a dielectric taking into account the long-range interaction, (2) the process is viewed in momentum space *quantifying the idea of velocity matching*, and (3) a semianalytic expression is derived using the Born approximation. From the resulting integral propensity rules are derived telling which final states are favored based on the initial target state and parameters of the collision. [S1050-2947(96)02008-2]

PACS number(s): 34.70.+e, 34.10.+x

I. INTRODUCTION

A large part of atomic research focuses on determining atomic structure and interactions with beam experiments. Atomic targets have been subjected to beams of electromagnetic radiation, light particles such as electrons, and heavier particles such as other atoms or ions. For electromagnetic beams, which are not too intense, induced atomic transitions are calculated assuming the dipole approximation for the electric vector of the radiation. The geometry of the various components in the dipole matrix element leads to selection rules telling which final states are accessible. For electron impact the wave function representing the incoming particles can be expanded in partial waves each of which allow transitions to a set of possible final states. A similar treatment for keV atomic collisions is impractical, as the harmonics necessary for accurate representation of the system number in the thousands [1]. Atomic collision systems instead lend themselves to a semiclassical approach which takes advantage of the near classical behavior of the atomic cores and treats the active electron quantum mechanically. Symmetry considerations do not restrict the number of available final states very much [2]; thus the concept of a propensity rule becomes useful to tell which of the many possible transitions are the most likely ones [3,4].

The need for an approximate integral, which gives the transition matrix for electron transfer in keV ion-atom collisions, has grown. Recent generations of beam experiments prepare target atoms to well-defined excited states through irradiation by coherent light of selected frequency and polarization [5]. In this article we concentrate on ion-atom collisions where the target atom is prepared in a low-*n* excited state. We focus on the range of projectile ion velocities near the average speed of the target atom's valence electron, since this is when the capture process is most significant. Experimentally, electron transfer in this type of system has been studied extensively [5]. Experiments show asymmetries in the capture cross sections from excited atomic *P* orbitals aligned parallel and perpendicular to the path of the projectile ions. In the case where differential cross section measurements are possible, capture asymmetry from states with opposite angular momentum orientation is measured. The corresponding calculations have had good agreement with the experiments [6]. Calculations based on a molecular or a two-center atomic description agree well with the measured asymmetry parameters, but the explanations of the underlying physical mechanisms are for the most part restricted to qualitative arguments.

To derive an expression for the amplitudes of charge transfer, we choose the two-center atomic basis approach, because the long-range limits are well represented. From the molecular point of view it is difficult to derive quantitative propensity rules, since rotational coupling mixes the molecular basis at long range. The atomic basis expansion has been used to find propensity rules for oriented targets [7,8]. Concepts that appear when discussing propensity rules for electron transfer are (1) energy defect between initial and final atomic states, (2) semiclassical impact parameter of the ion trajectory, (3) geometry of initial and final states, and (4) velocity-matching. The last concept is one that is unique to the capture process; the idea is that the capture probability increases if the current flow of the target's valence electron matches the speed of the passing ion. An attempt to quantify this idea was suggested in Ref. [9], where it is stated that the total capture probability should be proportional to an overlap of initial and final states in momentum space with the final state shifted by the projectile's velocity. This simple model displayed the same behavior as the experimentally measured asymmetry parameter for capture from aligned atoms. The shortcomings of this model are that it is not derived but postulated, it does not include energy defect, and it is a zero impact parameter model.

Based on the empirical success of this model, we decided to derive a more comprehensive model from the semiclassical atomic basis approach by expressing the matrix elements of this theory in momentum space. In the literature this has been a recurring theme in the attempt to understand electron transfer. The original formulation of the Born approximation for this process was expressed as an integral in momentum space [10]. Also some molecular approaches were formulated in momentum space [11,12]. The remainder of the article shows the derivation and predictions of a general propensity rule that includes the concepts of the preceding paragraph and encompasses alignment and orientation effects.

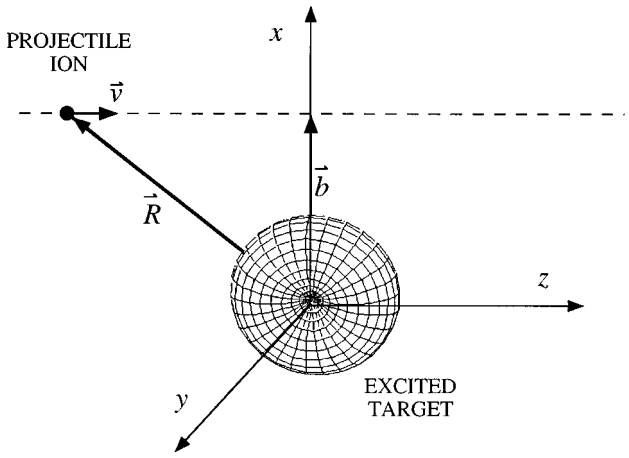

FIG. 1. Schematic of the ion-atom interaction shown in the collision frame. $\vec{R}$ is the internuclear vector, $\vec{b}$ is the classical impact parameter, and $\vec{v}$ is the projectile velocity.

II. GENERAL THEORY

We now go into more detail about electron transfer in atomic collisions represented by a two-center basis. The relative motion between the heavy particles is viewed classically, and the outcome of a collision is obtained as a function of initial position and velocity of the two atomic centers. The eikonal method [1] then gives the quantum mechanical differential cross sections by combining the different paths of the atoms, keeping track of the relative phases of the involved electronic states along the various atomic trajectories. The electronic motion is treated fully quantum mechanically with a further simplification that the projectile ion moves on a straight line past the target atom. This is quite a good approximation for keV atomic collisions. The Schrödinger equation for an electron in the field of the target and projectile nuclei in the rest frame of the target is (in a.u.)

$$i\frac{\partial}{\partial t}\Psi=\left(-\frac{1}{2}\nabla^2-\frac{Z_T}{|\vec{r}|}-\frac{Z_P}{|\vec{r}-\vec{R}|}\right)\Psi, \tag{2.1}$$

$$\vec{R}(t)=\vec{b}+\vec{v}t. \tag{2.2}$$

A schematic of this process with the pertinent parameters is given in Fig. 1. Throughout this article we use atomic units. Note that this means that the momentum of the electron and the velocity have the same dimensions, because $m_e=1$.

With the two-center basis the wave function for the active electron is expanded in atomic orbitals about both nuclei:

$$\Psi=\sum_m a_m\Psi_{T,m}+\sum_n b_n\Psi_{P',n}, \tag{2.3}$$

$$\Psi_{P'}\equiv e^{i[\vec{v}\cdot\vec{r}-(1/2)v^2t]}\Psi_P(\vec{r}-\vec{R}). \tag{2.4}$$

Ψ_T and Ψ_P are atomic orbitals centered on the target and projectile nuclei, respectively, and the subscript P' refers to the projectile atomic functions in the rest frame of the target. The coefficients a_m and b_n give the amplitude of each of the atomic functions. The exponential factor in Eq. (2.4) is the so-called electron translation factor (ETF) that is needed for the projectile atomic functions to have the correct momentum and energy in the target frame [1]. The advantage of this approach is that boundary conditions are simple to apply, since prepared target states and captured final states are atomic in nature. The drawbacks are added complications due to the ETF and nonorthogonality of the basis, when the overlap of target and projectile states becomes significant.

A. Atomic functions in momentum space

We write the transformation to momentum space, since this will play a large role in clarifying many aspects of the electron capture process,

$$\Phi(\vec{p})=\frac{1}{(2\pi)^{3/2}}\int_V e^{-i\vec{p}\cdot\vec{r}}\Psi(\vec{r})d\vec{r}, \tag{2.5}$$

$$\Phi_{P'}=e^{-i[\vec{R}\cdot\vec{p}-(1/2)v^2t]}\Phi_P(\vec{p}-\vec{v}). \tag{2.6}$$

In momentum space the velocity of the projectile states is a simple translation while the separation of the target and projectile is encoded in the new ETF shown in Eq. (2.6).

Just from comparing the projectile basis functions in configuration space, Eq. (2.4), and momentum space, Eq. (2.6), one can see immediately that the momentum space picture can prove fruitful. In configuration space the projectile functions all have nontrivial time dependence, because they are centered about the point indicated by $\vec{R}$. In momentum space this time dependence is transferred to the ETF, where it is more accessible to analytic treatment, as will be shown in Sec. III B. In configuration space the collision process occurs in a volume of space which can be hundreds of atomic units in extent because of the long-range forces involved. In momentum space the extent of the interaction region is around 5 a.u., since we are interested in relative velocities on the order of one or less a.u. The large distances are still, however, reflected in the rapid oscillation of the ETF, but the effect of these oscillations can be understood and dealt with in a simple manner (see Sec. III B).

B. Parabolic Coulomb functions

When examining the charge transfer process in an atomic collision, there is not only the problem of understanding the capture process itself, but also disentangling it from excitation of the atomic state on one center by the charge of the other center. As an ion approaches a target atom the electric field from the ion affects the target state long before the ion is in range to capture the electron, especially for the case of hydrogenic atoms, where each n manifold is degenerate. One can, however, incorporate most of this long-range excitation into the definition of the atomic basis on each center.

An example of an analytic treatment of the long-range forces in a charge transfer process is shown in work by Lundsgaard and Nielsen for capture from ground state hydrogen by an α particle. They found that they could significantly reduce the range of their calculation by using Stark states as a boundary condition [13]. Here, we follow up on this idea and include part of the linear term of the ionic Coulomb field in the atomic basis functions.

The Schrödinger equations which define the atomic basis on the target and projectile are

$$i\frac{\partial}{\partial t}\Psi_T=\left(-\frac{1}{2}\nabla^2-\frac{Z_T}{|\vec{r}|}+V_0^P(t)+E^P(n^T,n_1^T,n_2^T;t)\right)\Psi_T, \tag{2.7}$$

$$i\frac{\partial}{\partial t}\Psi_{P'}=\left(-\frac{1}{2}\nabla^2-\frac{Z_P}{|\vec{r}-\vec{R}|}+V_0^T(t)+E^T(n^P,n_1^P,n_2^P;t)\right)\Psi_{P'}. \tag{2.8}$$

The discussion proceeds only with Eq. (2.7), since both equations are defined in a symmetric way. The two extra terms, V_0^P and E^P, are only *time* dependent, representing a shift in energy due to part of the Coulomb interaction with the projectile ion. The V_0^P term is a uniform shift in the target atom's energy while the E^P term is a shift from the linear electric field in the z direction which depends on the shape of the target state. They are defined as follows:

$$V_P\equiv-\frac{Z_P}{|\vec{r}-\vec{R}(t)|}=V_0^P(t)+V_z^P(t)z+V_x^P(t)x\cdots, \tag{2.9}$$

$$E^P(n^T,n_1^T,n_2^T;t)=\frac{3}{2}V_z^P(t)\frac{n^T}{Z_T}(n_1^T-n_2^T). \tag{2.10}$$

V_P has no linear term in the y direction, because the potential is symmetric about the collision plane. Spatially Eqs. (2.7) and (2.8) are still hydrogenic, but it is intended that the spatial wave functions should be the parabolic Coulomb functions, since they are eigenstates of the linear Stark effect.

The shape of the specific basis functions is determined by the quantum numbers n,n_1,n_2. n still is the principal quantum number, but n_1 and n_2, which count the number of nodes in the ξ ($\xi=r+z$) and η ($\eta=r-z$) directions, respectively, replace the usual l and m of spherical coordinates [14]. The general basis state is written

$$\Psi_{T(P)}=f_{n,n_1,n_2}(\xi,\eta,\phi)e^{-i\phi_{T(P)}(t)}. \tag{2.11}$$

f is a parabolic Coulomb function which is a linear combination of the spherical Coulomb functions of the same n and m, where $|m|=n-n_1-n_2-1$, given in Ref. [14]. The time-dependent terms from Eqs. (2.7) and (2.8) enter into the phase of the basis functions analytically:

$$\phi_{T(P)}(t)=-\frac{1}{2}\frac{Z_{T(P)}^2}{(n^{T(P)})^2}t+\int_0^t V_0^{P(T)}(\tau)d\tau+\int_{-\infty}^t E^{P(T)}(\tau)d\tau$$
$$=-\frac{1}{2}\frac{Z_{T(P)}^2}{(n^{T(P)})^2}t-\frac{Z_{P(T)}}{v}\left(\ln\left[\frac{vt}{b}+\sqrt{1+\left(\frac{vt}{b}\right)^2}\right]\mp\frac{3}{2}\frac{n^{T(P)}(n_1^{T(P)}-n_2^{T(P)})}{Z_{T(P)}\sqrt{b^2+(vt)^2}}\right). \tag{2.12}$$

The initial point for the time integration of $V_0^{P(T)}$ is chosen to be zero for convenience. This choice does not affect the results here, because this phase is common to all of the capture atomic states. However, the integration of $E^{P(T)}$ must begin at $\tau=-\infty$, since it depends on the quantum numbers of the atomic state.

Including the extra terms, $V_0^{P(T)}$ and $E^{P(T)}$, in Eqs. (2.7) and (2.8) dramatically reduces the interaction region for ion-atom collisions for two reasons. First, the long-range effect of an ion on an atom is the linear electric field along the collision axis. Second, the $E^{P(T)}$ breaks the l degeneracy of the usual spherical atomic states. The m degeneracy is still present, but the long-range linear electric field is acting along the trajectory of the projectile ion, thus it cannot cause an m transition. With the reduction of interaction range it becomes easier to make a sensible first order analysis of the electron capture process itself.

C. The coupled equations

With the new basis defined the coupled equations governing the evolution of atomic state amplitudes follow from substitution of Eq. (2.3) into Eq. (2.1). In matrix form the coupled equations are

$$i\mathbf{S}\dot{\vec{a}}=\mathbf{M}\vec{a}, \tag{2.13}$$

where

$$\vec{a}\equiv\begin{pmatrix}a_m\\ b_n\end{pmatrix}, \tag{2.14}$$

$$\mathbf{S}\equiv\begin{pmatrix}\delta_{m',m} & \langle\Psi_{T,m'}|\Psi_{P',n}\rangle\\ \langle\Psi_{P',n'}|\Psi_{T,m}\rangle & \delta_{n',n}\end{pmatrix}, \tag{2.15}$$

$$\mathbf{M}\equiv\begin{pmatrix}\langle\Psi_{T,m'}|V_P-V_0^P-E_m^P|\Psi_{T,m}\rangle & \langle\Psi_{T,m'}|V_T-V_0^T-E_n^T|\Psi_{P',n}\rangle\\ \langle\Psi_{P',n'}|V_P-V_0^P-E_m^P|\Psi_{T,m}\rangle & \langle\Psi_{P',n'}|V_T-V_0^T-E_n^T|\Psi_{P',n}\rangle\end{pmatrix}. \tag{2.16}$$

(The subscripts m and n indicate which elements are summed in the matrix-vector multiplication.) These coupled equations closely resemble those of Refs. [1,7]. Taking into account part of the long-range interaction does not alter the structure of the coupled equations, but these extra terms subtracted from the interaction serve to increase the range of validity for a first order approximation.

There are three principal matrix elements that comprise Eq. (2.13): the overlap of target and projectile wave functions, the excitation interaction, and the electron transfer interaction. The matrix **S** in most multichannel treatments is the unit matrix, because one usually chooses orthonormal channel wave functions. Here, however, **S** has the unit matrix on the diagonal subblocks and the overlap of projectile

and target wave functions on the off-diagonal subblocks. This is the price for having atomic orbitals on two centers. The interaction matrix **M** represents two processes: excitation of the atomic orbital on one center by the potential of the other center, and the actual electron transfer process. The effect of the excitation interaction has a much reduced range, because much of the interaction is included in the basis functions Eqs. (2.7) and (2.8). The remainder can be evaluated efficiently by a multipole expansion of the projectile potential about the target atom, but this is left to a subsequent article. Since we are interested in examining the electron capture process, we go into further detail with the transfer matrix element.

The off-diagonal submatrices of **M** are responsible for charge transfer. The lower left subblock dictates when the electron jumps from target to ion, and there is also the possibility for transfer back to the target through the upper right subblock. The return of the electron from the projectile is not important for a first order theory, but it is definitely an important part of the full treatment. Writing out the general term $\mathbf{M}^{PT}$ for electron capture from the target atom, one obtains

$$\langle \Psi_{P',n}|V_P - V_0^P - E_m^P|\Psi_{T,m}\rangle$$

$$= \int_V \Psi_{P,n}^*(\vec{r}-\vec{R},t)e^{-i[\vec{v}\cdot\vec{r}-(1/2)v^2t]}[V_P(\vec{r},t)-V_0^P(t) - E_m^P(t)]\Psi_{T,m}(\vec{r},t)d\vec{r}. \quad (2.17)$$

The integrand is the product of the target wave function, the projectile wave function shifted in position by $\vec{R}$, the projectile's ETF, and the interaction due to the Coulomb field of the ion. The capture matrix element is rather complex, but upon transformation to momentum space it becomes possible to understand how the various parameters of the collision affect the capture probability.

To write the transfer integral in momentum space one inserts the δ function in the form of

$$\delta(\vec{r}-\vec{r}') = \frac{1}{(2\pi)^3}\int_{V_P} e^{-i\vec{p}\cdot\vec{r}}e^{i\vec{p}\cdot\vec{r}'}d\vec{p} \quad (2.18)$$

into the electron transfer integral. Placing it between the projectile potential and the target wave function performs the transformation to momentum space in the most efficient way. One of the exponentials acts forward to Fourier transform the target wave function, and the other works backward to transform the product of the projectile potential and the projectile wave function. This is straightforward to evaluate, since the potential energy can be written, using Eq. (2.8), as the difference of the total energy and the kinetic energy—a mere quadratic in momentum space. (Note that this avoids the usual problem with momentum space formulations which is that in general the Fourier transform of a product results in a convolution integral.) Equation (2.17) is equivalent to

$$\langle \Psi_{P',n}|V_P - V_0^P - E_m^P|\Psi_{T,m}\rangle$$

$$= \int_{V_P} \Phi_{P,n}^*(\vec{p}-\vec{v},t)e^{i[\vec{R}\cdot\vec{p}-(1/2)v^2t]} \times\left(\omega_n^P - \frac{1}{2}|\vec{p}-\vec{v}|^2 - V_0^P - E_m^P\right)\Phi_{T,m}(\vec{p},t)d\vec{p}, \quad (2.19)$$

where ω_n^P is the energy eigenvalue of the projectile state n.

The electron exchange integral written in the form of Eq. (2.19) starts to resemble the model in Ref. [9] in that there is an overlap of momentum space wave functions separated by $\vec{v}$. The remainder of the integrand must be understood to arrive at the new velocity matching. We will investigate the role of the ETF. We will also account for time dependence entering through the phase of the basis functions, the term V_0^P and the internuclear separation $\vec{R}$. The result will be a model for electron transfer that shows how the various parameters of this process affect the capture probability.

III. DERIVATION OF VELOCITY-MATCHING MODEL

Section II summarizes a complete semiclassical theory for electron capture in an ion-atom collision for relative velocities on the order of a couple atomic units or less. The process itself depends on many aspects such as impact parameter and velocity, geometry of target and projectile wave function, and energy defect between initial and final state. This section derives an approximate model for capture, where the impact velocity is near the average speed of the target's valence electron, which includes the effects of all these parameters in an intuitive way and is easy to calculate.

A. First-order approximation

The general ion-atom collision is a rather complicated process. The electron can be exchanged and undergo excitation on either center many times before reaching its final state. However, it will be seen for the range of velocity and impact parameter of interest here that it is a good approximation to consider only the direct transfer from the initial target state to a final capture state.

The information about the capture probability is contained in the coefficients b_n in Eq. (2.3). These coefficients are calculated by integrating $\dot{b}_n$, which must be extracted from the coupled differential equations (2.13). Multiplying on the left by $\mathbf{S}^{-1}$ untangles the $\dot{a}_m$'s from the $\dot{b}_n$'s. The inverse of **S**, to first order, is

$$\mathbf{S}^{-1} \approx \begin{pmatrix} \delta_{m',m} & -\langle \Psi_{T,m'}|\Psi_{P',n}\rangle \\ -\langle \Psi_{P',n'}|\Psi_{T,m}\rangle & \delta_{n',n} \end{pmatrix}. \quad (3.1)$$

The validity of this approximation depends on two factors. The number of atomic states to which the collision interaction is confined determines the rank of the matrices in Eq. (2.13), and as the rank of **S** grows the worse the approximation in Eq. (3.1) becomes. The magnitude of the off-diagonal

matrix elements of **S**, namely, the overlap between target and projectile states, is also relevant.

Since the magnitude of the overlap matrix elements is a key factor for the approximations made in this section, it is important to know their dependence upon the various collision parameters. Explicitly the integrals for the overlap between target and projectile atomic states, expressed in configuration and momentum space, are

$$\langle \Psi_{P'}|\Psi_T\rangle = \int_V \Psi_P^*(\vec{r}-\vec{R},t)e^{-i[\vec{v}\cdot\vec{r}-(1/2)v^2t]}\Psi_T(\vec{r},t)d\vec{r} = \int_{V_p} \Phi_P^*(\vec{p}-\vec{v},t)e^{i[\vec{R}\cdot\vec{p}-(1/2)v^2t]}\Phi_T(\vec{p},t)d\vec{p}. \tag{3.2}$$

From Eq. (3.2) one can see that the magnitude of the overlap matrix elements decreases with either increasing impact parameter or velocity. The size of the overlap between a projectile and a target state also depends on the principal quantum number of the particular atomic states considered; the extent of an atomic orbital in configuration space is n^2/Z and in momentum space it is Z/n. These expressions provide a criterion for the range of impact parameter and velocity where a first order theory can be expected to work.

We now employ the Born approximation by fixing the coefficient of the initial target state to unity and the others to zero in the state vector on the right side of Eq. (2.13). This results in a first order expression for both the excitation and capture amplitudes. Focusing on the capture amplitudes, the time derivative of the expansion coefficients for the projectile along its trajectory is

$$\dot{b}_n \approx i\sum_{m''} \langle \Psi_{P',n}|\Psi_{T,m''}\rangle\langle \Psi_{T,m''}|V_P - V_0^P - E_{m_0}^P|\Psi_{T,m_0}\rangle - i\langle \Psi_{P',n}|V_P - V_0^P - E_{m_0}^P|\Psi_{T,m_0}\rangle. \tag{3.3}$$

The contribution to electron capture comes through two terms, the second of which is the transfer integral discussed in Sec. II C.

The first term in Eq. (3.3) represents the leading order molecular effect as the projectile ion forms a temporary complex with the target atom. We will, however, neglect this term, since the basis is chosen such that the excitation is small and the overlap integral is already assumed small. Hence this term is considered as a second order effect. To first order the time derivative of the capture coefficients is

$$\dot{b}_n = -i\langle \Psi_{P',n}|V_P - V_0^P - E_{m_0}^P|\Psi_{T,m_0}\rangle + \cdots. \tag{3.4}$$

Equation (3.4) appears in Chapter 10 of Ref. [1], but the derivation, here, in terms of a truncated basis is necessary for showing the range of validity of the velocity-matching model. The time integration of Eq. (3.4) follows in the next section, to obtain a formula for the capture amplitudes themselves.

B. The window function

The usual way to proceed from Eq. (3.4) is to evaluate the matrix element on the right-hand side and then to integrate in time. We will instead perform the time integration first. This requires that the time dependence be separated from the integration variables of the matrix element. This will not work with the configuration space version of $\mathbf{M}^{PT}$ in Eq. (2.17), since the projectile wave function and potential depend on $\vec{R}$ which in turn depends on time. On the other hand, the capture matrix element evaluated in momentum space, Eq. (2.19), is much more suited to this type of analysis.

The momentum space transfer integral has only one factor where the integration coordinate $\vec{p}$ and time t are tied together: the ETF. This factor, $e^{i\vec{R}\cdot\vec{p}}$, indicates the position of the projectile, and we can write it as the product $e^{ibp_x}e^{ivtp_z}$ in the collision frame, see Fig. 1. The phase of the second exponential contains the product of time and the momentum coordinate p_z. Thus the integration of the matrix element (2.19) in time amounts to a Fourier transformation from time to the frequency $-vp_z$ which is directly proportional to p_z due to the assumption of constant velocity.

The time dependence in Eq. (2.19) enters from three factors: V_0^P and E^P, the phase of the basis functions in Eq. (2.12), and the ETF. Rewriting Eq. (3.4) with the momentum space transfer integral Eq. (2.19) and explicitly showing all time dependence, it becomes

$$\dot{b}_n \approx -i\int_{V_P} O_{PT}I_P e^{-i[\Delta\omega+(1/2)v^2]t}e^{ivtp_z}d\vec{p}, \tag{3.5}$$

$$O_{PT} \equiv \Phi_{P,n}^*(\vec{p}-\vec{v})\Phi_{T,m_0}(\vec{p})e^{ibp_x}, \tag{3.6}$$

$$I_P \equiv \omega_n^P - \frac{1}{2}|\vec{p}-\vec{v}|^2 + \frac{Z_P}{\sqrt{b^2+(vt)^2}} + \frac{3}{2}\frac{Z_P vtn^T(n_1^T-n_2^T)}{Z_T[b^2+(vt)^2]^{3/2}}, \tag{3.7}$$

$$\Delta\omega \equiv \frac{\phi_T(t)-\phi_P(t)}{t}. \tag{3.8}$$

The ETF is split up in order to partition the integrand in three basic factors. The first, Eq. (3.6), is an overlap of target and projectile momentum space wave functions including the time-independent part of the ETF. The second term, Eq. (3.7), is the interaction due to the projectile potential in which only the last two terms vary in time. The last term, Eq. (3.8), is the energy defect between projectile and target states.

Up until now the exact time dependence has been kept in the formulation for completeness. However, we will now eliminate terms involving the gradient of the projectile potential in the z direction, $E^{T(P)}$, since they are a factor of $|\vec{R}|$ less important than the zeroth order terms, $V_0^{T(P)}$. Specifically, the last terms of Eqs. (2.12) and (3.7) are removed. This may seem as if we are defeating the purpose of going to parabolic Coulomb functions, but these basis functions are still useful, because they are closer to the eigenstates of the interaction causing excitation. The next section clarifies this point.

The dependence of the energy defect term is still complicated by the logarithmic terms in the phase of the basis functions, Eq. (2.12). To simplify this expression we approximate the phase by a line with a slope determined by evaluating the logarithmic terms at a distance a from the target defined as an interaction range for capture [15]:

$$\phi_{T(P)}(t) \approx (\omega_n^{T(P)} + \omega_c^{P(T)})t, \tag{3.9}$$

$$\omega_c^{P(T)} \equiv \frac{Z_{P(T)}}{a} \ln\left[-\frac{a}{b} + \sqrt{1+\left(\frac{a}{b}\right)^2} \right]. \tag{3.10}$$

The interaction range a replaces vt in Eq. (2.12). For the calculations presented in this article it is set to 25 a.u., but the slope in Eq. (3.9) is not sensitive to this parameter. ω_c^P represents the energy by which the target state is lowered due to the field of the projectile ion averaged over the interaction region. Thus we approximate the energy defect by

$$\Delta\omega_{\rm lin} = \omega_{m_0}^T - \omega_n^P + \omega_c^P - \omega_c^T. \tag{3.11}$$

Note that the target and projectile charges have to be unequal for the logarithmic terms to contribute to the energy defect.

With the approximations to the phase dependence of the basis it is possible to integrate analytically both sides of Eq. (3.5) in time. Performing the time integration inside the momentum space integral will give a window function in p_z which is centered around a momentum of $\Delta\omega_{\rm lin}/v + v/2$. Since the first two terms of I_P in Eq. (3.7) are independent of time, their window is a Dirac δ function. In the third term time appears in the square root. Fourier transforming this expression gives a zeroth order modified Bessel function of the second kind with a width in momentum of $1/b$. This type of Bessel function is similar to a decaying exponential, since it is the transform of the square root of a Lorentzian. We wish to find a model for large impact parameter, so we take this latter window to be a δ function also. This δ function receives the proper normalization through multiplication by the area of the true window function.

After time integration using the approximations mentioned above we reach the velocity-matching model for electron transfer. The expression for the capture coefficients is

$$b_n \approx -i\frac{2\pi}{v}\int_{V_P} O_{PT}\left(\omega_n^P - \frac{1}{2}|\vec{p}-\vec{v}|^2 + \frac{Z_P}{b}\right) \times \delta\left(p_z - \frac{\Delta\omega_{\rm lin} + \frac{1}{2}v^2}{v}\right) d\vec{p}. \tag{3.12}$$

Numerical evaluation of this integral is not difficult, considering that it is only a two-dimensional integral and that it is sufficient to take a range of a few atomic units in each direction. The rapid oscillations alluded to in Sec. II A disappeared with the time integration. The structure of the integral in Eq. (3.12) leads to propensity rules for the electron transfer amplitudes. Also, we present an alternative, related derivation which appeals more to the physical intuition of charge transfer.

C. Propensity rules

The symmetries of Eq. (3.12) lead to general predictions for the electron capture process. The velocity-matching model preserves the reflection symmetry about the collision plane, which stems from the original Hamiltonian Eq. (2.1) [1,2]. Another symmetry emerges by having written Eq. (3.12) in terms of parabolic Coulomb functions in momentum space. It predicts that the final state of the captured electron will have no dipole in the direction of the projectile velocity. The last general consequence of Eq. (3.12) occurs at a particular relative velocity between the ion and atom, where the velocity-matching model shows extreme state selectivity.

The velocity-matching model predicts that there should be no net z dipole for the final state in electron capture from a spherical atomic state. However, this is a propensity rule, since it derives from Eq. (3.12), which is an approximate result. This follows from a property of the parabolic Coulomb functions in momentum space:

$$\Phi_{n_1,n_2,m}(\vec{p}) = (-1)^{n+m-1}\Phi^*_{n_2,n_1,-m}(\vec{p}). \tag{3.13}$$

Even though a parabolic state may have an asymmetric probability distribution in configuration space upon reflection in the xy plane, it is completely symmetric in momentum space upon reflection in the $p_x p_y$ plane [15]. From Eq. (3.13) the integral in Eq. (3.12) gives amplitudes, equal in magnitude, upon exchange of n_1 and n_2 for either the target or projectile state, provided that the other state is a spherical Coulomb function. For the example we choose in the results section, Sec. IV, we consider capture from atomic hydrogen prepared in various $2P$ states, thus the final state can have a dipole only in the x direction.

For the discussion of the next point we switch to the spherical Coulomb functions, because their angular dependence is identical in momentum and configuration space. The next interesting result of Eq. (3.12) occurs for a particular projectile velocity called the crossover velocity, which is defined

$$v_c \equiv \sqrt{2|\Delta\omega_{\rm lin}|}. \tag{3.14}$$

As the ion velocity scans through v_c, the window function crosses over $p_z = 0$, the midplane of the target momentum distribution (if $\Delta\omega_{\rm lin}$ is negative), or $p_z = v$, the midplane of the projectile momentum distribution (if $\Delta\omega_{\rm lin}$ is positive). Since the window function is a δ function, the integral in Eq. (3.12) is automatically zero unless the atomic state, over which the window is centered, has positive reflection symmetry in the xy plane (the equivalency of momentum and configuration space angular functions is used here). This property, in combination with the reflection symmetry about the collision plane, has a dramatic effect on the state selectivity of the velocity-matching model for projectile velocities near v_c as will be seen in Sec. IV B.

D. Interpretive model

In this section we present another expression for the capture amplitudes which provides a clear physical insight into the mechanism of charge transfer around the matching ve-

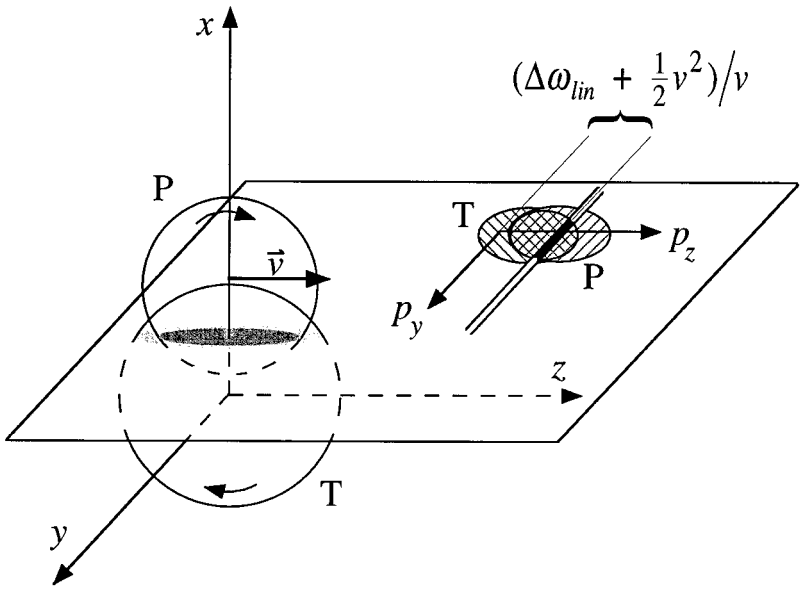

FIG. 2. Schematic of the integral for the interpretive velocity-matching model. The displayed plane is at a constant and arbitrary value of x. Schematically the wave function cross sections are shown in configuration space on the lower left corner of the plane and in momentum space on the upper right corner. The window function is also shown, and the area which is completely black shows the contribution to the capture integral.

locity. The starting point for the alternative derivation is Eq. (3.4) where the time derivative of the capture coefficients is given by the transfer integral in Eq. (2.17). Instead of completely switching this integration from one over configuration space variables to one over momentum space variables, it will be expressed as a mixed integration, where two of the degrees of freedom are momenta and one is a position. The resulting expression is not practical for calculation, but gives a clear picture of how the various parameters of the collision process affect the outcome.

Rewriting Eq. (2.17), explicitly making use of the collision coordinate frame and the expansion of the projectile potential in Eq. (2.9), it becomes

$$\langle \Psi_{P',n}|V_P - V_0^P - E_m^P|\Psi_{T,m}\rangle$$

$$\approx \int_V \Psi^*_{P,n}(x-b,y,z-vt,t)e^{-i[vz-(1/2)v^2t]} \times V_x^P(t)x\Psi_{T,m}(x,y,z,t)d\vec{r}, \tag{3.15}$$

$$V_x^P(t) = \frac{-Z_P b}{[b^2+(vt)^2]^{3/2}}. \tag{3.16}$$

In this form of the capture integral the projectile potential is expanded around the target position to first order. The zeroth order term cancels against V_0^P as it was designed to do, and the linear term cancels against V_z^P under the assumption that this term does not mix the n shells of the target atom. Replacing the y and z integration variables by p_y and p_z, an alternative expression for the time derivative of the capture amplitudes appears:

$$\dot{b}_n \approx -i \int_{V_{\text{mixed}}} O_{PT}^{\text{alt}} I_P^{\text{alt}} e^{-i[\Delta\omega+(1/2)v^2]t} e^{ivtp_z} dx\ dp_y dp_z, \tag{3.17}$$

$$O_{PT}^{\text{alt}} \equiv \Xi^*_{P,n}(x-b,p_y,p_z-v)\Xi_{T,m_0}(x,p_y,p_z), \tag{3.18}$$

$$I_P^{\text{alt}} \equiv \frac{-Z_P bx}{[b^2+(vt)^2]^{3/2}}. \tag{3.19}$$

At this point once again the time integration is performed.

With the linear form of the energy defect $\Delta\omega_{\text{lin}}$ it is possible to integrate Eq. (3.17) analytically. The interaction I_P^{alt} transforms to a Bessel function once again, but to obtain a more illuminating formula, we cancel the impact parameter b in the numerator of Eq. (3.19) against one of the powers of $|\vec{R}|$ in the denominator:

$$I_P^{\text{alt}} \sim \frac{-Z_P x}{b^2+(vt)^2}. \tag{3.20}$$

This approximation gives an exponential for the window function. The capture coefficients are thus given by

$$b_n \approx i\frac{\pi Z_P}{bv}\int_{V_P} xO_{PT}^{\text{alt}} e^{-b|p_z-[\Delta\omega_{\text{lin}}+(1/2)v^2]/v|} dx\ dp_y dp_z. \tag{3.21}$$

This form of the velocity-matching model is not well suited for calculation, since the wave functions in this mixed space can only be found numerically. Also Eq. (3.12) takes into account the projectile potential to all orders while Eq. (3.21) is based on a linear expansion of the potential. But it is a good guide for the intuition to see the outcome of the electron transfer process.

The velocity-matching model presented in Eq. (3.21) gives a clear picture of how the state-to-state capture probability depends on various parameters of the collision. Figure 2 shows schematically the different components that go into the integral. The principal interaction driving the capture process is the perpendicular electric field from the projectile ion, thus the term $Z_P x/b$ appears in the integral. The phase factors due to the ETF have been converted into a separation b in the x coordinate and v in the p_z momentum coordinate. The exponential window only allows momenta which counterbalance the excess momentum $\Delta\omega_{\text{lin}}/v + v/2$ gained by the electron upon transfer to an atomic orbital about the pro-

jectile nucleus. The width of the window in momentum, $1/b$, reflects the fact that a wider range of energy defects can be accommodated as the charge center of the projectile ion passes closer to the target atom, since the ion's Coulomb potential energy at the target center sweeps through a broader range.

The concept of velocity-matching is well formulated mathematically as an overlap in the mixed space of Eq. (3.21). A velocity-matching model should not only account for when the electron probability current matches on the target and capture states, but should see where the currents match at *common points in configuration space*. As shown in Fig. 2, the localization in configuration space comes with the integration over the x coordinate, which is perpendicular to the direction of the projectile motion. The probability currents of the target and projectile states in each plane of constant x are then compared by the integration in momentum space. Since Eq. (3.21) is well suited for interpretation, we will use it in combination with the propensity rules of the preceding section for understanding the results calculated by Eq. (3.12).

IV. RESULTS

Having developed a first order theory for electron capture in an ion-atom collision, we choose a particular system on which to test it. We wanted to examine a pure three body Coulombic system having an asymmetry in the nuclear charge, to test also the shift in energy defect due to Eq. (3.10). Thus we selected the system: α particle incident on an excited hydrogen atom. Other theoretical calculations for this system are given in Refs. [16,17]. In this section the results of the velocity-matching model are compared with results obtained from the program used in Ref. [13], modified to calculate capture from excited target atoms [18].

We are interested in studying capture for the range of projectile velocities near the average speed of the valence electron of the hydrogen target. Since we look at capture from hydrogen excited to the $n=2$ shell, the ''matching'' velocity is 0.5 a.u. . From either Eq. (3.12) or Eq. (3.21) one can find out immediately which n shells on the α particle will be significantly populated by the capture process. Figure 3 shows the location of the window function in p_z as a function of projectile velocity for capture states in the first three n shells. The positions of projectile and target are indicated for reference. For the range of velocities we are interested in clearly the $n=3$ shell will dominate over the other two, because the corresponding window function moves into the region between the projectile and target. Comparing the results of the velocity-matching model with the more complete theoretical calculation for electron transfer from $H(n=2)$ to $He^+(n=3)$ allows us to test the model for a system where the capture process is the dominant one.

A. Alignment and orientation

Experiments measuring electron transfer in ion-atom collisions with excited targets have been primarily concerned with the dependence of the capture cross section on the geometry of the excited target state. Thus in this section we display the norm of the capture amplitudes into the

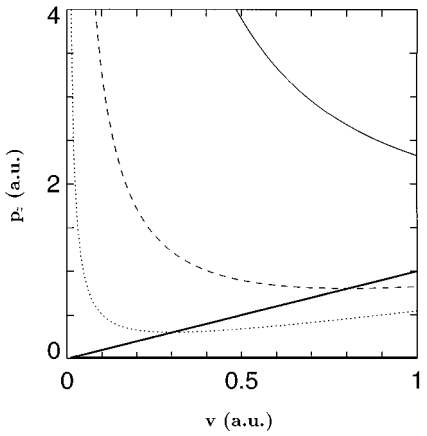

FIG. 3. Position of the window function in p_z as a function of v. The solid curve is for capture into $He^+(n=1)$, the dashed curve is for $n=2$, and the dotted curve is for $n=3$. All curves were calculated for an impact parameter of $b=15$ a.u.

$He^+(n=3)$ as a function of projectile velocity, impact parameter, and initial $H(2P)$ alignment and orientation. We do not, however, compare at the level of cross sections, since this requires integration over impact parameter and for low impact parameter the overlap between target and projectile wave functions is not necessarily small, invalidating one of the assumptions in Sec. III A.

The initial states considered here have positive reflection symmetry with respect to the collision plane, meaning that the initial P state is aligned in the collision plane and has average angular momentum perpendicular to the collision plane. To describe the initial states, we label aligned states according to which axis in the collision frame (see Fig. 1) the alignment is parallel. A P_x state is aligned perpendicular to the incoming ion beam, and a P_z state is aligned along the projectile beam velocity. For oriented states we label according to the angular momentum component in the direction perpendicular to the collision plane: $P_{l_y=1}$ and $P_{l_y=-1}$ refer to orbitals rotating counterclockwise and clockwise, respectively, when seen from the positive y axis.

For the purpose of discussion Fig. 4 displays contour plots

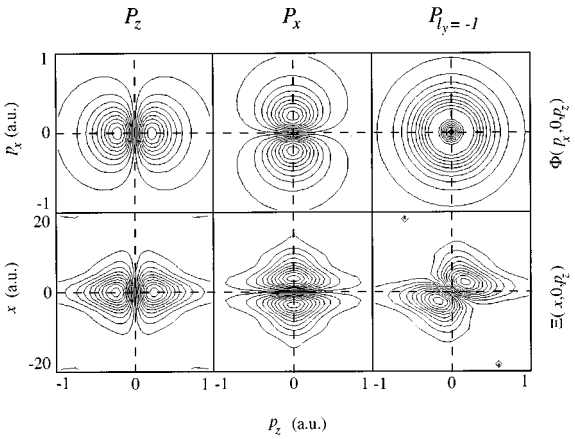

FIG. 4. Contour plots of the $p_y=0$ cross section for some initial target states. The top row shows the states in momentum space, while the bottom row shows them in the mixed space.

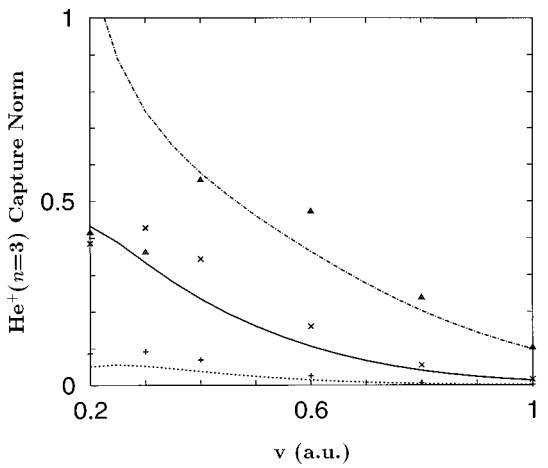

FIG. 5. Total capture into the $He^+(n=3)$ from a P_z initial state. The chain curve displays the model results for $b=10$ a.u., the solid curve is for $b=15$ a.u., and the dotted curve is for $b=20$ a.u. The triangles show points of the close coupled calculation for $b=10$ a.u., the crosses are for $b=15$ a.u., and the plus signs are for $b=20$ a.u.

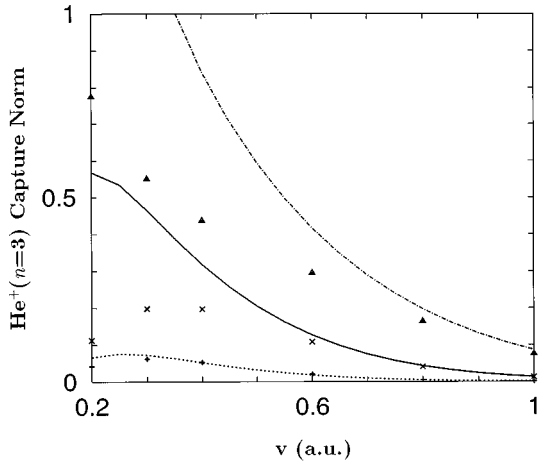

FIG. 6. Total capture into the $He^+(n=3)$ from a P_x initial state. The chain curve displays the model results for $b=10$ a.u., the solid curve is for $b=15$ a.u., and the dotted curve is for $b=20$ a.u. The triangles show points of the close coupled calculation for $b=10$ a.u., the crosses are for $b=15$ a.u., and the plus signs are for $b=20$ a.u.

of these initial states in momentum space and the mixed space of Sec. III D. It must be borne in mind that the interpretive model not only includes the overlap of projectile and target wave functions in the mixed space, but also a window in p_z with a width $\approx 1/b$ and a center indicated in Fig. 3.

1. Aligned target states

Figure 5 shows the results for the norm of capture into $He^+(n=3)$ from an initial $H(2P)$ state aligned along the collision velocity. For large impact parameter, $b=20$ a.u., the model follows the points from the close coupled calculation, but there is a gap in the magnitude of the two theories. This difference comes from having neglected molecular effects in the expression from the capture amplitude [i.e., neglecting the first term on the right-hand side of Eq. (3.3)]. For the smaller impact parameters of $b=10$,15 a.u., where the capture norm is a significant fraction of unity, the velocity-matching model achieves similar agreement. There is deviation of the model away from the close coupled calculation for $b=10$ a.u. and $v<0.4$ a.u., but this is to be expected since the overlap between the target and projectile atomic functions becomes too large.

Figure 6 displays the norm of capture into the $He^+(n=3)$ from an initial $H(2P)$ state aligned perpendicular to the collision velocity. Again the agreement is good for either $b>10$ a.u. or $v>0.4$ a.u., and when the overlap of target and projectile wave functions becomes large, the velocity-matching model diverges away from the results of the more extensive calculation. In comparison with the capture amplitude from the P_z initial state capture from the P_x falls off faster as a function of projectile velocity in both the model and close coupled calculations. This general trend can be understood by looking at the initial states in the mixed space, Fig. 4. The P_x state decays at a quicker rate than the P_z state as the z component of the momentum increases. The difference in electron transfer for oriented initial states is more dramatic.

2. Oriented target states

Looking at the amplitude for electron transfer from the $P_{l_y=1}$ initial state to the $He^+(n=3)$ in Fig. 7, there are remarkable differences from the results of the preceding section. First of all the amplitude for capture is much reduced from the case of electron transfer from the aligned P orbitals. Furthermore, the velocity-matching model predicts substantially lower amplitudes than the close coupled calculation, especially around the matching velocity. The low capture norm predicted by the model is seen by examining the oriented state shown in Fig. 4.

The state in the figure has $l_y=-1$, but the distribution for $l_y=1$ is the same upon reflection about the $x=0$ line. A collision of this target state with a projectile moving with

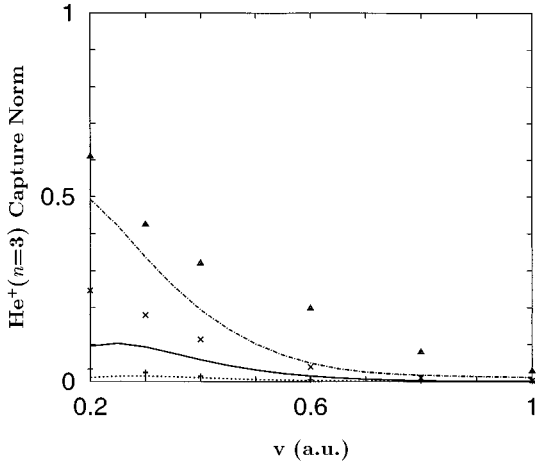

FIG. 7. Total capture into the $He^+(n=3)$ from a $P_{l_y=1}$ initial state. The chain curve displays the model results for $b=10$ a.u., the solid curve is for $b=15$ a.u., and the dotted curve is for $b=20$ a.u. The triangles show points of the close coupled calculation for $b=10$ a.u., the crosses are for $b=15$ a.u., and the plus signs are for $b=20$ a.u.

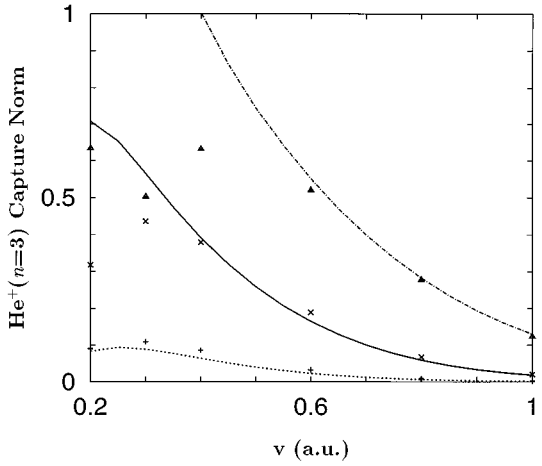

FIG. 8. Total capture into the $He^+(n=3)$ from a $P_{l_y=-1}$ initial state. The chain curve displays the model results for $b=10$ a.u., the solid curve is for $b=15$ a.u., and the dotted curve is for $b=20$ a.u. The triangles show points of the close coupled calculation for $b=10$ a.u., the crosses are for $b=15$ a.u., and the plus signs are for $b=20$ a.u.

$v=0.5$ a.u. at an impact parameter $b=10$ a.u. corresponds to centering the projectile at the exact middle of the fourth quadrant ($p_z>0$ and $x<0$) of the oriented state in Fig. 4. One can see, however, that this state has little probability for entering the fourth quadrant, hence the low values in evaluating the electron transfer integral. The model thus quantifies the intuitive idea that the amplitude for capture is low when the projectile ion hits on the side of the oriented state where the electron current flows *against* the velocity of the projectile. The fact that the velocity-matching model underestimates the capture amplitude around the matching velocity comes from neglecting excitation of the target state. If excitation were included, the target could evolve into a state with a component more favorable to electron transfer. This process is included in the close coupled calculation, and this results in the larger amplitudes around $v=0.5$ a.u. for capture from the $P_{l_y=1}$ initial state. For the initial state oriented in the opposite sense the situation is quite different.

Figure 8 shows the capture norm from the $P_{l_y=-1}$. The capture amplitude is larger, and the agreement between the close coupled calculation and the velocity-matching model is better. Visualizing the velocity-matching integral with Fig. 4 amounts to centering the projectile in the first quadrant ($p_z>0$ and $x>0$) in the mixed space plot of the oriented state. This orbital has a peak in the first quadrant, stating that the electron current flows in the direction of the projectile ion on the same side of the target that the projectile passes by. The direct capture is clearly favored for this initial state, hence the good agreement of the velocity-matching model with the extended calculation.

B. State-to-state amplitudes

The velocity-matching model also gives the final state that the electron is captured into. We show only the final state of the $He^+(n=3)$ after capture from the $P_{l_y=-1}$ initial H($2P$) state, since the final states for capture from the aligned orbitals are not much different from this case. The final state for capture from $P_{l_y=1}$ shows disagreement between the velocity-matching model and the close coupled calculation near projectile velocities of $v=0.5$ a.u., because the main contribution to capture for this case comes through target states induced as the projectile ion approaches.

TABLE I. The magnitude of final-state amplitudes calculated by the velocity-matching model (VMM) and the close coupled calculation (CCC) for $b=15$ a.u. and $v=0.4$ a.u. The amplitudes are coefficients of the parabolic atomic basis for $He^+(n=3)$.

(m,n_1,n_2)	$\lvert b^{\mathrm{VMM}}_{m,n_1,n_2}\rvert$	$\lvert b^{\mathrm{CCC}}_{m,n_1,n_2}\rvert$
(−2,0,0)	0.1138	0.0926
(−1,0,1)	0.1380	0.1442
(−1,1,0)	0.1380	0.1210
(0,0,2)	0.0978	0.1337
(0,1,1)	0.1787	0.1699
(0,2,0)	0.0978	0.0939
(1,0,1)	0.1380	0.1442
(1,1,0)	0.1380	0.1210
(2,0,0)	0.1138	0.0926

To show a comparison at the level of the state-to-state amplitudes, we list the final state amplitudes from both the velocity-matching model and the extended calculation for capture from $P_{l_y=-1}$ at an impact parameter, $b=15$ a.u., and velocity, $v=0.4$ a.u. Table I displays the final state amplitudes in terms of coefficients of the parabolic atomic basis. There are symmetries that are apparent upon inspection of this table. First, the magnitudes are the same for m and $-m$ for both the model and the extended calculation. This comes from the reflection symmetry of the Hamiltonian and initial state in the collision plane. Second, the amplitudes for the model are the same upon interchange of n_1 and n_2. As discussed in Sec. III C and reflected in the numbers of Table I, this property is only approximate in the close coupled calculation.

To illustrate the dependence of the final state on projectile velocity and impact parameter and to give a more clear picture of the final state itself, we select a set of independent observables [19]. We calculate the dipole moment, orientation, and alignment of the final state. Due to reflection symmetry through the collision plane the dipole moment in the y direction is zero, and the angular momentum is directed perpendicular to the collision plane; $\langle D_y\rangle=0$ and only $\langle L_y\rangle$ can be nonzero. The symmetry under exchange of n_1 and n_2 for the velocity-matching model implies that there is no dipole component in the z direction; $\langle D_z\rangle=0$. Alignment of the final state is revealed by plotting $\langle L_x^2\rangle$ and $\langle L_z^2\rangle$. Roughly speaking the ''thickness'' of the orbital as seen from the x direction is proportional to $\langle L_x^2\rangle$. Only results for $b=15,20$ a.u. are shown. For lower impact parameters, $b=10$ a.u., the final state predicted by the model loses its meaning due to modification from the field of the stripped target. All displayed observables are shown with the ordinate spanning the whole range of possible values for the $He^+(n=3)$ shell.

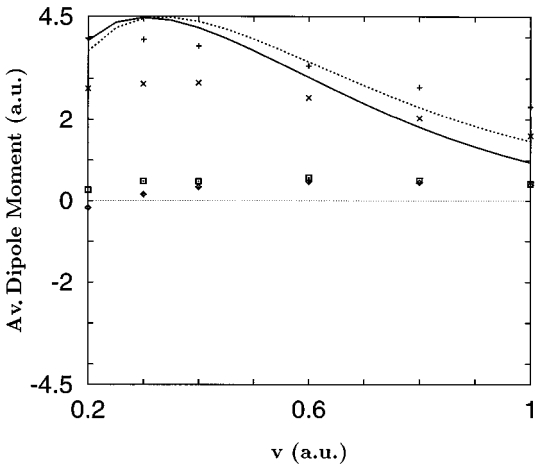

FIG. 9. $\langle \vec{D} \rangle$ for $He^+(n=3)$. The solid curve shows the model results of $\langle D_x \rangle$ for $b=15$ a.u. and the dotted curve is for $b=20$ a.u. The crosses show $\langle D_x \rangle$ calculated from the amplitudes of the close coupled calculation for $b=15$ a.u. and the plus signs are for $b=20$ a.u. Also shown is $\langle D_z \rangle$ for the close coupled calculation ($\langle D_z \rangle$ for the velocity matching is not displayed, since it is zero). The boxes represent points for $b=15$ a.u. and the diamonds are for $b=20$ a.u.

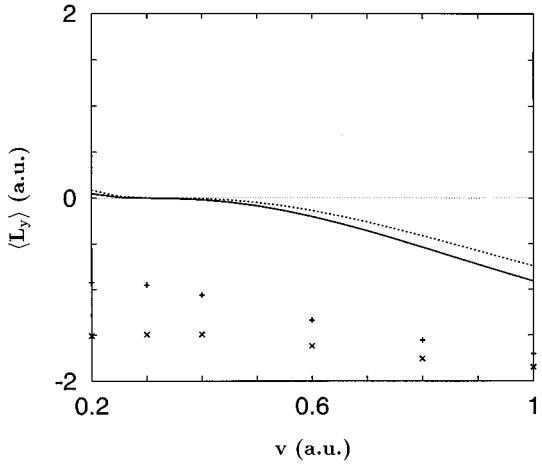

FIG. 10. $\langle L_y \rangle$ for $He^+(n=3)$. The solid curve shows the model results for $b=15$ a.u. and the dotted curve is for $b=20$ a.u. The crosses show $\langle L_y \rangle$ calculated from the amplitudes of the close coupled calculation for $b=15$ a.u. and the plus signs are for $b=20$ a.u.

Figure 9 shows the dipole moment of the final state. The predicted dipole in the x direction by the velocity-matching model is quite large, achieving nearly the maximum possible value slightly above $v=0.3$ a.u. The average electron position (which is the negative of the dipole) points toward the target atom. Reaching the maximum value for $\langle D_x \rangle$ means that the final state is nearly a pure parabolic Coulomb function with the quantization axis perpendicular to the projectile velocity. As for the comparison with the close coupled calculation the large value and trend of $\langle D_x \rangle$ are reproduced. The extended calculation shows only a small dipole in the z direction, which agrees with the propensity rule of Sec. III C. The total dipole of the final state is well described by the velocity-matching model.

Looking at the angular momentum in Fig. 10, we see quite a discrepancy between the prediction of the model and the points of the extended calculation. The downward trend in the angular momentum is reproduced in the model, but there is a substantial offset. The model crosses zero angular momentum precisely at the point where the maximum dipole is predicted. Also at this velocity $\langle L_x^2 \rangle$ is zero, see Fig. 11, indicating that the final state is completely aligned along the x axis. For such a state if a small component aligned along the z axis is added with the proper phase, the angular momentum can deviate from zero quite strongly. As one can see in Fig. 11 the close coupled calculation shows a small component aligned along the z axis, but it is large enough to cause the deviation in the angular momentum. The value of $\langle L_z^2 \rangle$ for the final state orbital seen in Fig. 12 shows a nearly constant value of 1 a.u. for both the velocity-matching model and the close coupled calculation. The final plot in Fig. 13 represents the square of the total angular momentum. The underestimation by the velocity-matching model is from the discrepancy in $\langle L_y \rangle$, and the trend toward the maximum value of $\langle L^2 \rangle$ reflects the increase in magnitude of $\langle L_y \rangle$.

The observables plotted in Figs. 9–13 paint a clear picture of the final state predicted by the velocity-matching model, which can be understood by the propensity rules of Sec. III C and the interpretive model Eq. (3.21). For capture into $He^+(n=3)$ the crossover velocity is 0.33 a.u. at an impact parameter of $b=20$ a.u., and v_c shifts down to 0.30 a.u. for $b=15$ a.u. From Sec. III C it is known that the projectile final state must have positive reflection symmetry in the xy plane at v_c. Due to the collision geometry the final state wave function must also have positive reflection symmetry in the xz plane (the collision plane). The only possible states obeying both symmetries have $m=0$, when the x axis is taken as the quantization axis. In the $n=3$ shell three states have $m=0$, namely, the S, P, and D states. To apply the

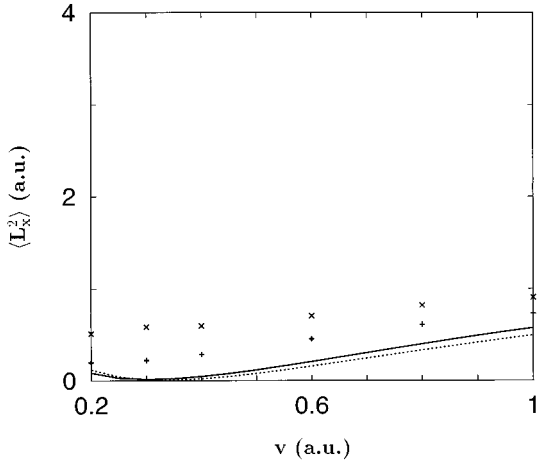

FIG. 11. $\langle L_x^2 \rangle$ for $He^+(n=3)$. The solid curve shows the model results for $b=15$ a.u. and the dotted curve is for $b=20$ a.u. The crosses show $\langle L_x^2 \rangle$ calculated from the amplitudes of the close coupled calculation for $b=15$ a.u. and the plus signs are for $b=20$ a.u.

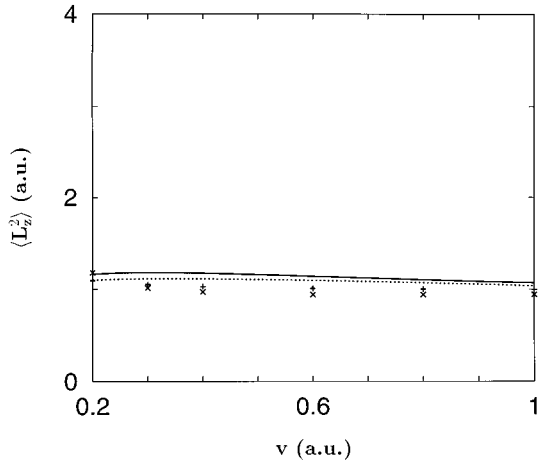

FIG. 12. $\langle L_z^2 \rangle$ for $He^+(n=3)$. The solid curve shows the model results for $b=15$ a.u. and the dotted curve is for $b=20$ a.u. The crosses show $\langle L_z^2 \rangle$ calculated from the amplitudes of the close coupled calculation for $b=15$ a.u. and the plus signs are for $b=20$ a.u.

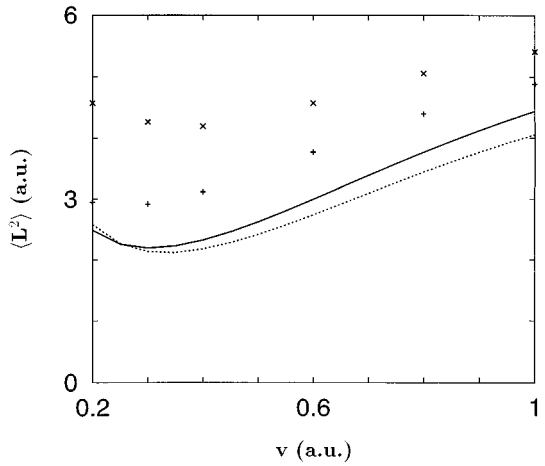

FIG. 13. $\langle L^2 \rangle$ for $He^+(n=3)$. The solid curve shows the model results for $b=15$ a.u. and the dotted curve is for $b=20$ a.u. The crosses show $\langle L^2 \rangle$ calculated from the amplitudes of the close coupled calculation for $b=15$ a.u. and the plus signs are for $b=20$ a.u.

interpretive model, it is more convenient to combine these three spherical wave functions into parabolic Coulomb eigenstates. Since Eq. (3.21) is an integral over the configuration space coordinate x, the parabolic state which points toward the target, in the x direction, is heavily favored. This explains the maximal dipole at the crossover velocity seen in Fig. 9. Moreover, at v_c the symmetry requirements prevent the final state from having a net angular momentum. As the velocity increases, the final capture state widens and gains angular momentum in the clockwise direction seen from above the collision plane. This increase in the angular momentum of the final state is explained by velocity-matching: as the projectile velocity increases, final states that have a backward current on the side closest to the target are favored.

V. CONCLUSION

The velocity-matching model presented in Eqs. (3.12) and (3.21) gives capture amplitudes for electron transfer in ion-atom collisions, where the relative velocity is on the order of the average velocity of the active electron. The results obtained by this model for intermediate impact parameters compare well to the solutions of the full close coupled differential equations (2.13) at the level of state-to-state amplitudes despite the fact that the velocity-matching model is much simpler. From the standpoint of calculation Eq. (3.12) is only a two-dimensional integration of well-behaved functions over a region on the order of 10×10 a.u.^{2} in momentum. On the other hand, to solve the close coupled equations requires evaluation of the time-dependent three-dimensional integrals of Eq. (2.13), and then subsequently integrating the coupled differential equations (2.13) in time.

Even though we have chosen to develop our formulation in terms of hydrogenic parabolic atomic functions, this model can still be applied to non-Coulombic atoms. We work with parabolic functions here for two reasons: the discrepancies between our model and the close coupled equations are limited to few states (see the fourth row of Table I) because of limitations on target excitation viewed in this basis, and also the propensity rule of equal capture probability into states with opposite z-dipole moment is revealed. Eliminating the last term of Eqs. (2.12) and (3.7) in Sec. III B removes the need to use parabolic functions. One could instead insert spherical wave functions generated from a model potential into Eq. (3.12). Thus the velocity-matching model is useful for making an exploratory calculation to reveal the general behavior of a particular charge transfer system, and to suggest which states are important for capture before bringing the full machinery of the close coupled equations to bear.

The velocity-matching model incorporates all the concepts known to be important to electron transfer and views the process in its most natural frame. The energy defect between initial and final states determines the position of the window in p_z. The impact parameter enters into the expression of the area of the window function, the strength of the electric field pulling the electron from the target, and of course the separation of target and projectile in x. The velocity affects the energy defect, and determines the separation of target and projectile in p_z. The geometry of initial and final states is reflected in their respective wave functions. Finally, the formulation as an integral over x, p_y, and p_z, Eq. (3.21), captures the essence of the concept of velocity matching.

ACKNOWLEDGMENTS

The authors wish to thank Svend Erik Nielsen and Nils Andersen for their support and helpful discussions. The first author also acknowledges the support of Grant No. D 930055 from the Danish Research Academy.

[1] B. H. Brandsen and M. R. C. McDowell, *Charge Exchange and the Theory of Ion-Atom Collisions* (Clarendon Press, Oxford, 1992), Chap. 3.
[2] N. Andersen, J. W. Gallagher, and I. V. Hertel, Phys Rep. **165**, 1 (1988).
[3] U. Fano, Phys. Rev. A **32**, 617 (1985).
[4] R. S. Berry, J. Chem. Phys. **45**, 1228 (1966), Sec. IV D.
[5] J. W. Thomsen *et al.*, J. Phys. B **28**, L93 (1995), references therein provide a comprehensive overview of capture from excited target atoms.
[6] T. H. Rod and S. E. Nielsen, J. Phys. B **28**, L607 (1995), see references therein.
[7] S. E. Nielsen, J. P. Hansen, and A. Dubois, J. Phys. B **23**, 2595 (1990).
[8] A. Dubois, J. P. Hansen, M. Lundsgaard, and S. E. Nielsen, J. Phys. B **24**, L269 (1991); E. E. B. Campbell, I. V. Hertel, and S. E. Nielsen, *ibid.* **24**, 3825 (1991); A. Dubois, S. E. Nielsen, and J. P. Hansen, *ibid.* **26**, 705 (1993).
[9] S. Schippers, A. R. Schlatmann, and R. Morgenstern, Phys. Lett. A **181**, 80 (1993).
[10] J. D. Jackson and H. Schiff, Phys. Rev. **89**, 359 (1953); H. C. Brinkman and H. A. Kramers, Proc. Acad. Sci. Amsterdam **33**, 973 (1930); N. Bohr, K. Dan. Vidensk. Selsk. Mat. Fys. Medd. **18**, No. 8 (1948).
[11] J. B. Delos and W. R. Thorson, Phys. Rev. A **6**, 720 (1972).
[12] M. S. Child, *Molecular Collision Theory* (Academic Press, London, 1974), see Appendix D.
[13] M. F. V. Lundsgaard and S. E. Nielsen, Z. Phys. D **34**, 97 (1995).
[14] L. D. Landau and E. M. Lifschitz, *Quantum Mechanics (Non-relativistic Theory)*, 3rd ed. (Pergamon Press, New York, 1977), Sec. 37.
[15] H-J. T. Simonsen, Master's thesis, Copenhagen University–Ørsted Laboratory, 1996.
[16] J. P. Hansen, S. E. Nielsen, and J. Schweinzer, J. Phys. B **26**, L471 (1993).
[17] B. D. Esry, Z. Chen, C. D. Lin, and R. D. Piacentini, J. Phys. B **26**, 1579 (1993).
[18] Svend Erik Nielsen provided us with a code that calculates electron transfer and excitation amplitudes for the He^{2+}-particle–H system with a 28-state atomic basis.
[19] R. Hippler, J. Phys. B **26**, 1 (1993).